FR9601639

CURRENT DRIVE EFFICIENCY REQUIREMENTS FOR AN ATTRACTIVE STEADY-STATE REACTOR

G. Tonon

Association EURATOM-CEA
DRFC/STID - Cadarache
13108 - St Paul Lez Durance - France

Abstract

We consider first, the expected values of the figure of merit γ and the electrical efficiency η_{CD} of various non-inductive current drive methods. After, we summarize the main experimental results achieved today, with neutral beams and radiofrequency systems. Taking into account the simplified energy flow diagram of a steady state reactor, we determine the figure of merit and the electrical efficiency values which are necessary in order to envisage an attractive steady-state reactor. These values are finally compared to the theoretical predictions.

I. Introduction

Commercially attractive tokamak fusion reactors will require steady state operation mainly because the thermal fatigue of key elements is reduced and the thermal energy storage is eliminated [1] [2]. These advantages of steady state operation should be balanced against the recirculating power needed to maintain the plasma current.

Consequently, for an attractive tokamak steady state reactor it is necessary to reduce as much as possible the amount of externally driven current I_{CD}. This necessitates mainly to minimize the plasma current I_p (high q_ψ operation) and to maximize the bootstrap current fraction (high poloidal beta β_p operation). In addition the reactor potential of the tokamak could be considerably improved if an efficient system, using a combination of various methods if necessary, of driving the plasma current could be developed and demonstrated. In order to build an attractive steady state tokamak reactor various parameters of the current drive system have to be improved. They are :

(i) The current drive figure of merit :

$$\gamma = \langle ne \rangle R I_{CD} / P_{CD}$$

where <ne> is the volume average electron density, R the major radius and P_{CD} the total injected power to drive the current I_{CD} .

(ii) The electrical efficiency $\eta_{CD} = P_{CD}/P_{ECD}$ where P_{ECD} represents the electrical power needed to supply the non inductive current drive system.

(iii) The capital cost figure of merit C_{CD} (ECU Watt) cf the non-inductive current system.

The scope of this paper is to compare the predictions concerning γ and η_{CD} for various non-inductive current drive methods to the values required in view to obtain an attractive steady state reactor. In Sec. II a survey of theoretical predictions concerning γ is presented and some experimental results are given. The expected electrical efficiencies η_{CD} are also discussed. The Sec. III summarize the steady state constraints obtained considering the power flow diagram of two tokamak reactor designs. The required γ and η_{CD} values and the comparison with their predicted values are considered in Sec. IV. Finally, in Sec. V some concluding remarks are given.

The units are mks with the plasma current in MA, power in MW, density in 10^{20} m^{-3} and temperature in 10 keV.

II. Survey of the figure of merit and electrical efficiency of some non-inductive current drive methods

We consider the following external current drive methods :

- neutral beams (NBCD),
- fast waves in the ion-cyclotron and low frequency range (FWCD),
- lower hybrid waves (LHCD),
- electron cyclotron waves (ECCD).

For these methods basic physic is well understood [3] and successful demonstration experiments have been performed.

II.1. Current drive figure of merit γ

(i) Considering p_{CD} the power density to drive the current density j_{CD} on the plasma, we introduce the following normalisations :

$$\begin{cases} \hat{j} = j_{CD} / n \cdot e \cdot v_e \\ \hat{p} = p_{CD} / n\, m_e\, v_e^2\, \nu_0 \end{cases} \qquad \begin{pmatrix} m_e = \text{electron mass} \\ n = \text{density} \end{pmatrix} \tag{1}$$

where $v_e = (kT_e/m_e)$ is the electron thermal velocity and $\nu_0 = \omega_{pe}^4 \,\mathrm{Log}\,\Lambda / 2\pi n v_e^3$ the collision frequency where ω_{pe} represents the electron plasma frequency. From (1) we have :

$$j_{CD} / p_{CD} \approx 10^{-1} \left(\frac{Te}{ne}\right) \left(\hat{j} / \hat{p}\right) \tag{2}$$

Considering flat profiles, the total power P_{CD} and the corresponding total driven current I_{CD} are given by :

$$\begin{cases} I_{CD} = \pi a^2 k \cdot j_{CD} \\ P_{CD} = 2\,\pi^2\, R a^2 k \cdot p_{CD} \end{cases} \tag{3}$$

From relations (2) and (3) we can now define a figure of merit :

$$\gamma = < ne > R\, I_{CD} / P_{CD} = 0.015\, T_e \left(\hat{j} / \hat{p}\right) \tag{4}$$

(ii) The dimensionless function $\left(\hat{j} / \hat{p}\right)$ is calculated for the various methods using 2D-Fokker Planck equation and taking into account of trapped electron and relativistic effects if necessary. For example for waves, $\left(\hat{j} / \hat{p}\right)$ is plotted on figure 1 as a function of the normalized phase speed $W = v_{ph}/v_e = C/N_{//} \cdot v_e$ ($N_{//}$ = parallel refraction index ; vph = phase velocity), considering the electron LANDAU damping (Fig. 1a) and the ALFVEN wave damping (Fig. 1b) [4]. On this figure 1, four different poloidal angles and various inverse aspect ratios values ε are used. We see that, on flux surfaces with a local inverse aspect ratio $\varepsilon > 0.1$ and normalized phase speed $W < 1$, trapped electrons reduce notably the $\hat{j} / \hat{p}$ value. On the other hand, the rôle of the relativistic effect is seen on figure 2 for the electron LANDAU damping. On this figure 2 we have indicated on the right-hand side the figure of merit and the $N_{//}$ - domain covered by today lower hybrid experiments is represented.

A simple algebraic expression, not including trapped particle effects, can be used [5] :

$$\hat{j} / \hat{p} = \frac{2D}{Z_{eff} W} + 2\left[1 + \frac{6(6 + Z_{eff})}{(5 + Z_{eff}(3 + Z_{eff}))}\right] + \frac{8W^2}{(5 + Z_{eff})} \tag{5}$$

where $D = 3.76$ for the LANDAU damping.

(iii) The calculated evolution of the figure of merit γ versus volume averaged electron temperature $<Te>$ for neutral beams, fast waves and lower hybrid waves, is plotted on figures 3a, 3b and 3c respectively. We note that in general γ increases with $<Te>$. On this paper we use the following approximate analytical expressions :

a) NBCD :

$$\gamma_{NB} = 0.25 < Te > \cdot F(Z_{eff}, Z_b, M_b) \tag{6a}$$

with :
$$F(Z_{eff}, Z_b, A_b) = 1 - \frac{Z_b}{Z_{eff}}\left[1 - \frac{1.46}{A^{1/2}} \cdot \left(1 + \frac{0.667}{Z_{eff}^{0.945}}\right)\right] \approx 1$$

where M_b, Z_b are the beam ion mass and charge and $A = R/a$ the aspect ratio. The optimum beam energy $E_b \approx (30 \text{ to } 50)\, M_b\, Te \approx 2$ MeV.

b) FWCD :

$$\gamma_{FW} \approx 0.63 < Te > /(2 + Z_{eff}) \tag{6b}$$

The frequency is chosen in order to avoid ion absorption ($f \sim 20$ MHz for ITER).

c) LHCD :

$$\gamma_{LH} \approx \frac{0.37}{(5 + Z_{eff})} \times \frac{B_T}{< ne >^{1/3}} \times < Te > \qquad (6c)$$

The $B_T / < ne >^{1/3}$ dependence is determined by the accessibility constraint :

$$N_{//} \geq N_{//ACC} \equiv \omega_{pe} / \omega_{Ce} + \left[1 + \omega_{pe}^2 / \omega_{Ce}^2 - \omega_{pi}^2 / \omega^2\right]^{1/2}$$

where ω_{Ce} represents the electron cyclotron frequency. In order to avoid the α-particle absorption it is necessary to use a high frequency ($\geq$ 5 GHz on ITER).

d) ECCD :

$$\gamma_{EC} \approx 0.9 < Te > /(5 + Z_{eff})$$

we have supposed $W \sim 3$ and that a single pass absorption is achieved.

II.2. Summary of the main experimental results

II.2.1. Lower hybrid waves :

(i) High L.H. driven currents have been achieved : 3.6 MA on JT60U [6], 1.8 MA on JET [7] and 1.6 MA on Tore Supra [8].

(ii) The highest experimental current drive figure of merit has been obtained on JET [9] using lower hybrid and ion cyclotron waves : $\gamma \approx 0.42\ 10^{20}$ m^{-2} MA/MW taking into account synergetic effects. We have $\gamma \approx 0.34\ 10^{20}$ m^{-2} MA/MW on JT60U [6] and $\gamma \sim 0.15$ to $0.2\ 10^{20}$ m^{-2} MA/MW on Tore Supra [8].

II.2.2. Fast waves :

(i) About 0.18 MA of current has been driven on DIIID [10] and 0.08 MA on Tore Supra [11]. These current are well predicted by theory.

(ii) The figure of merit γ lies between 0.02 to $0.03\ 10^{20}$ m^{-2} MA/MW.

II.2.3. Electron cyclotron waves :

(i) Experiments on DIIID have found currents of 0.1 MA driven by electron-cyclotron waves [10]. Good agreement is obtained between the Fokker-Planck code and the experiment.

(ii) the best value of the figure of merit $\gamma \sim 0.016\ 10^{20}$ m^{-2} MA/MW is observed on DIIID [10].

II.2.4. Neutral beams :

On TFTR $\gamma \sim 0.05\ 10^{20}$ m^{-2} MA/MW while on TEXTOR $\gamma \sim 0.052$ when neutral beams are combined with ion-cyclotron heating [12].

II.3. Electrical efficiency η_{CD}

II.3.1. Radiofrequency systems

The general diagram of a radio frequency (RF) system is shown on figure 4a. Then the electrical efficiency η_{CD} is given by :

$$\eta_{CD} = \eta_{HV} \cdot \eta_{GEN} \cdot \eta_{TRANS}$$

where η_{HV}, η_{GEN} and η_{TRANS} are the high voltage power supply efficiency, the generator efficiency and the transmission efficiency respectively. On table I we have indicated for the three RF methods, the various efficiencies. For each of them, two values are given (i) a probable value which can be obtained with a small development from existing techniques (ii) a possible value which necessitates a strong development ; for example the utilisation of the depressed collector technique increases the tube efficiency as indicated by the following relation :

$$\eta_{TUBE} = \frac{\eta_{RF}}{1 - \eta_C(1 - \eta_{RF})}$$

where η_C is the collector recovery efficiency and η_{RF} the tube efficiency without the degreased collector.

II.3.2. Neutral Beams

The diagram of a neutral beam system is represented on figure 4b. The electrical efficiency, neglecting the power dissipated in the ion source and for pumping, is roughly given by :

$$\eta_{CD} \approx \frac{\eta_{ACC} \cdot \eta_{TRANS} \cdot \eta_N}{1 - \eta_R(1 - \eta_N)\eta_{ACC}}$$

where η_{ACC}, η_{TRANS}, η_N are the acceleration, transmission and neutralization efficiencies respectively and η_R the recovery efficiency. The neutralization efficiency in the gas cell is 0.60 , while in the plasma cell it reaches 0.8. Considering $\eta_{TRANS} \approx 0.8$ and $\eta_{ACC} \approx 0.85$ and without energy recovery we have :

(i) a probable electrical efficiency (with a gas neutraliser) : $\eta_{CD} \approx 0.4$,

(ii) a possible electrical efficiency (if a plasma neutralizer available) : $\eta_{CD} \approx 0.5$.

TABLE 1

	FWCD		LHCD		ECCD	
	Probable	Possible	Probable	Possible	Probable	Possible
η_{HV}	0.95	0.95	0.95	0.95	0.9	0.95
η_{GEN}	0.72	0.85	0.60	0.70*	0.35	0.50*
η_{TRANS}	0.88	0.88	0.85	0.90	0.85	0.85
η_{CD}	0.6	0.7	0.5	0.6	0.27	0.40
FREQUENCY	50 MHz		5 to 8 GHz		200 to 300 GHz	

* with depressed collector.

III. STEADY STATE REACTOR

III.1. Power balance

We consider the general power flow diagram shown in figure 5. The fusion neutron power P_{FN} increased by the blanket energy multiplication M and a fraction f of the alpha-particle power $P_{F\alpha}$ and the current drive power P_{CD}, assumed to appear as high-grade heat usable by the thermal cycle, compose the thermal power P_{TH} :

$$P_{TH} = M.P_{F\alpha} + f\,(P_{f\alpha} + P_{CD})$$

This thermal power is converted to the gross electric power $P_{EG} = \eta_T.P_{TH}$ with a thermal conversion efficiency η_T. The net electric power $P_{EN} = P_{EG}\,(1 - \varepsilon_C)$ is supplied to the grid where $\varepsilon_C = P_{EC}/P_{EG}$ represents the recirculating power fraction. In the recirculating power $P_{EC} = P_{CD} + P_{AUX}$, the power necessary for the auxiliary systems P_{AUX} (cryogenics, pumping power, etc.) represents a fraction $\eta_{AUX} = P_{AUX}/P_{EG}$ of the gross electric power. With these conditions, the net electric power is equal to :

$$P_{EN} = \eta_T(1-\eta_{AUX})\left(M+\frac{f}{4}\right)P_{FN}\left\{1-\frac{(\varepsilon_C-\eta_{AUX})[1-\eta_T\eta_{CD}(1-\eta_{AUX})f]}{(1-\eta_{AUX})[1-\eta_T\eta_{CD}(\varepsilon_C-\eta_{AUX})]f}\right\} \qquad (7)$$

and the plasma power multiplication factor :

$$Q = \frac{(P_{FN}+P_{F\alpha})}{P_{CD}} = \frac{1.25[1-\eta_T\eta_{CD}(\varepsilon_C-\eta_{AUX})f]}{\eta_T\eta_{CD}(\varepsilon_C-\eta_{AUX})\left(M+\frac{f}{4}\right)} \qquad (8)$$

Figure 6 shows the evolution of Q as a function of the recirculating power fraction ε_C for $\eta_T = 0.4$ and various values of η_{CD}. We see the strong influence of ε_C on Q : low Q values are associated with a high recirculating power.

III.2. Plasma model

We use a O-D simplified plasma power balance (Te = Ti) with profiles of the form $\rho_i = \rho_{i0}\,(1 - x^2)^{\alpha i}$ where $x = r / a$; the peaking factors for density and temperature are respectively $\alpha_n = 0.5$ and $\alpha_t = 1$.

The energy confinement time is given by :

$$\tau_E = H\,.\,\tau_{E\ ITER\text{-}89P} \qquad (9)$$

where H represents the confinement time multiplier factor.

The DT fusion reactivity is approximate by the following expression :

$$\langle\sigma_v\rangle_{DT} = 1.1\ 10^{-22}\ T^2 \qquad (10)$$

The plasma current is given by :

$$I_p = I_{CD} + I_{BS} \qquad (11)$$

where I_{BS} represents the bootstrap current. The bootstrap fraction $\chi = I_{BS} / I_p$ is evaluated as follows :

$$\chi = J_{BS}\,\beta_p / 2A^{1/2} \qquad (12)$$

where β_p is the poloidal beta value and J_{BS} a numerical factor depending on profiles : we take $J_{BS} = 1.2$.

The safety factor q_ψ is given by :

$$q_\psi = \frac{5aB_T(117 - 0.65/A)}{A(1 - 1/A^2)^2 I_p} \times \left[\frac{1 + K^2(1 + 2\delta^2 - 1.2\delta^3)}{2}\right] \qquad (13)$$

where the triangularity $\delta = 0.3$.

The total toroidal beta value β must satisfy the following constraint :

$$\beta = \beta_N \frac{I_p}{a \cdot B_T} \qquad (\%) \qquad (14)$$

with the dependence of the Troyon factor given by the ARIES-I correlation [13] :

$$\beta_N = \frac{2.8\left[1 - 0.4(K-1)^2\right]}{(1 - 1/A)^{3/2}} \qquad (15)$$

The H factor is calculated so that the toroidal beta is determined by the relations (14) and (15).

III.3. Technical constraints-Design points

(i) The internal structure thickness Δ_{INT} (shield + blanket + first wall + gaff) is supposed given roughly by $\Delta_{INT} = R / 5$. Consequently the peak magnetic field B_{TM} on the inboard leg of the superconducting toroidal coil is related to the toroidal magnetic field on plasma axis B_T by the following relation :

$$B_{TM} = B_T / (0.8 - 1/A) \qquad (16)$$

Otherwise we take $M = 1.25$; $f = 0.7$ and $\eta_{AUX} = 0.065$.

(ii) We consider a class of reactor delivering a net electrical power $P_E = 1000$ MW with a recirculating power fraction $\varepsilon_C = 0.2$. In order to maximize the bootstrap current fraction we take $A = 4.5$ and $q_\psi = 5$. A moderate elongation $K = 1.75$ is used.

(iii) We have selected two designs :

- R1 (classical design) : the peak magnetic field $B_{TM} = 13$ Teslas and water cooling is retained giving $\eta_T = 0.35$;
- R2 (advanced design) : the peak magnetic field $B_{TM} = 18$ Teslas and He cooling is envisaged giving $\eta_T = 0.47$. This design is similar to the SSTR [14] and ARIES-I [15] designs.

For R2, the main parameters are summarized in Table 2. In this advanced design R2 , the plasma current is moderate $I_p \sim 10$ MA and we can realise a high bootstrap current fraction $\alpha \sim 70$ %. The necessary confinement time multiplier $H \sim 2.3$ is equivalent to the values achieved to day in the advanced regimes at a comparable $\beta_p/A \sim 0.5$ value.

TABLE 2 : R2 Parameters

• Aspect ratio A = R/a	4.5
• Major toroidal radius R(m)	6.53
• Plasma minor radius a(m)	1.45
• Elongation K	1.75
• Plasma edge factor q_ψ	5
• Plasma current I_p(MA)	9.2
• Peak TF-coil magnetic field B_{TM}(T)	18
• On-axis toroidal magnetic field B_T(T)	10.4
• Bootstrap current fraction χ	0.62
• Current drive power P_{CD}(MW)	78
• Confinement time multiplier H_{ITER89}	2.35
• Plasma poloidal beta β_p	2.2
• Troyon coefficient β_N	0.031
• Gross electric power P_{EG}(MW)	1250
• Net electric power P_{EN}(MW)	1000
• Recirculating power fraction ε_C	0.2

IV. REQUIRED γ AND η_{CD} VALUES AND COMPARISON WITH PREDICTIONS

The evolution of the product $\langle ne \rangle . \langle T \rangle$ as a function of B_{TM} is shown in figure 7 ; we have :

- design R1 : $\langle ne \rangle . \langle T \rangle \approx 1.2\ 10^{21}\ m^{-3}$ keV
- design R2 : $\langle ne \rangle . \langle T \rangle \approx 2.3\ 10^{21}\ m^{-3}$ keV.

On this figure is also indicated the evolution of the triple product $\gamma \langle T \rangle \eta_{CD}$ for the two values of the thermal efficiency η_T. We see that for a given design $\gamma \langle T \rangle \eta_{CD}$ is constant. In the figure 8, we have represented the evolution of $\gamma\, \eta_{CD}$ as a function of the average temperature $\langle T \rangle$ for R1 and R2. It appears that for :

- $\langle T \rangle$ = 10 keV : a value of $\gamma . \eta_{CD} = 0.4\ 10^{20}\ m^{-2}$ MA/MW is necessary for R1 and $0.32\ 10^{20}\ m^{-2}$ MA/MW for R2 ;
- $\langle T \rangle$ = 15 keV : a value of $\gamma . \eta_{CD} = 0.26\ 10^{20}\ m^{-2}$ MA/MW is required for R1 and $0.22\ 10^{20}\ m^{-2}$ MA/MW for R2.

But, as indicated before, our plasma model implies that the toroidal beta is fixed and, consequently $\gamma . \eta_{CD} / \langle ne \rangle$ is also constant as shown in figure 9. We note that for $\langle ne \rangle = 10^{20}\ m^{-3}$ it is necessary that :

- $\gamma . \eta_{CD} \approx 0.32\ 10^{20}\ m^{-2}$ MA/MW for R1,
- $\gamma . \eta_{CD} \approx 0.14\ 10^{20}\ m^{-2}$ MA/MW for R2.

On the other hand, the predicted evolution of $\gamma.\eta_{CD}$ as a function of the electron density for each non-inductive current drive method is determined considering :

(i) the approximate analytical expressions (6a) to (6 d),

(ii) the electrical efficiency η_{CD} given in paragraph II.3.

(iii) the <ne>.<T> values indicated in figure 7 for R1 and R2.

The results are shown in figures 10a and 10b for the R1 and R2 designs respectively. The required $\gamma.\eta_{CD}$ values are obtained when the predicted $\gamma.\eta_{CD}$ values satisfied the reactor requirements also indicated in the figures.

We see that we have approximately the same values for R1 and R2 :

- LHCD : $\gamma_{LH}\,\eta_{LH} \approx 0.3\ 10^{20}\ m^{-2}$ MA/MW
- NBCD and FWCD : $\gamma_{NB}\,\eta_{NB} \approx \gamma_{FW}\,\eta_{FW} \approx 0.2\ 10^{20}\ m^{-2}$ MA/MW
- ECCD : $\gamma_{EC}\,\eta_{EC} \approx 0.12\ 10^{20}\ m^{-2}$ MA/MW.

But the required $\gamma.\eta_{CD}$ values for each non-inductive current drive method are obtained for different plasma operating parameters as shown in figure 11. In the <ne>, <T> domain, we have indicated the plasma operating points for each non-inductive current drive method. With the R2 design, we can work at higher electron-densities which are more in line with the divertor constraints. The LH wave penetration can be a problem at high density, in spite of the high magnetic field value (see Table 2) [14]. For the EC waves the operating temperature seems to high, especially taking into account our approximate expression (10) for the DT fusion reactivity which overestimate the fusion power.

V. CONCLUDING REMARKS

With an advanced reactor design (similar to the ARIES-I and SSTR designs) it is possible to obtain a steady state regime using non-inductive current drive methods in conjunction with a high bootstrap current fraction (~ 70 %).

The electrical efficiency of these non-inductive current drive methods plays a key role. Considering the present state of the art it appears (except perhaps for the fast wave method) that an aggressive development programme is necessary.

A strong experimental programme concerning combined scenarios (LH + ICRH, FW + ECRH, NB + ICRH, LH + ECRH, etc.) has to be undertaken in view to increase (i) the flexibility of the current drive system (ii) the current profile control capability [16] (iii) the current drive figure of merit γ through synergetic effects [9].

Complete non-inductive powerful steady state discharges (pulse length exceeding many resistive diffusion and particle saturation wall times) have to be produced in order to study practical means to control simultaneously the total plasma current and its profile. This kind of discharges can be produced on Tore Supra Continu, TPX and JT60.SU.

References

[1] D.A. EHST et al.
Nuclear Engineering and Design/Fusion 2 (1985), p. 305-318.

[2] C.G. BATHKE and the ARIES Research Team 18th Symposium on Fusion Technology, August 1994, Karlsruhe - Germany.

[3] N.J. FISH.
Rev. Mod. Phys. Vol. 59 n° 1 (1987), p. 175.

[4] D.A. EHST and C.F.F. KARNEY.
Nuclear Fusion, Vol. 31 N 10 (1991), p. 1933.

[5] D.A. EHST, K. EVANS Jr.
Nuclear Fusion, Vol. 27 N 8 (1987), p. 1267.

[6] O. NAITO and the JT60 Team.
Plasma Phys. Control. Fusion 35 (1993) B 215.

[7] C. GORMEZANO.
Private communication.

[8] Equipe Tore Supra presented by G. TONON.
Plasma Phys. Control. Fusion 35 (1993) A105.

[9] C. GORMEZANO et al
IAEA Tech. Com. Meeting on Fast Wave Current Drive in Reactor Scale Tokamak.
Arles, France, 1991, p. 245.

[10] R. PRATER et al.
GA-A 21525, February 1994.

[11] Equipe Tore Supra presented by B. SAOUTIC.
21st E.P.S. Montpellier, France, 1994, to be published.

[12] A. MESSIAEN et al.
Ibid 9, p. 334.

[13] Y.K.M. PENG et al.
IEEE Thirteenth Symp. on Fusion Engineering.
Knoxwille, 1989, Vol. 2, p. 1279.

[14] M. KIKUCHI
Ibid [6] p. B39.

[15] R.W. CONN, F. NAJMABADI.
Thirteenth Int. Conf. on Plasma Phys. and controlled Nuclear Fusion Research.
Washington DC, October 1990, IAEA CN 53/H.1.4.

[16] D. MOREAU.
This conference.

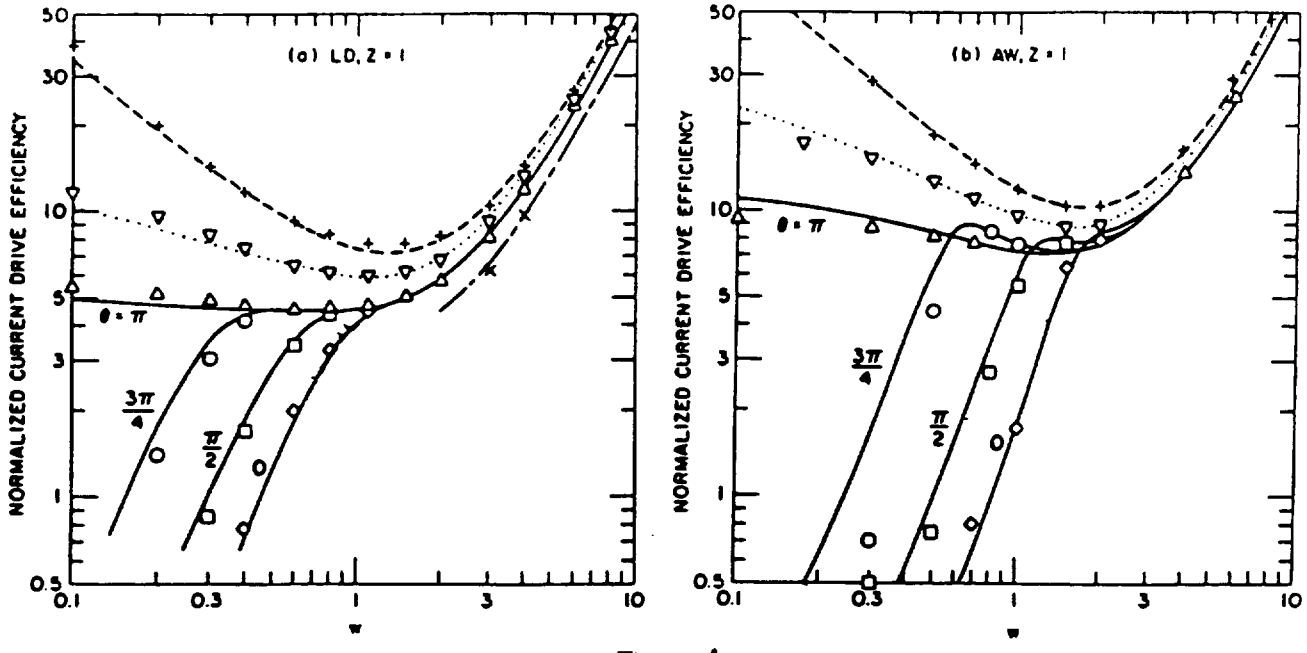

Figure 1

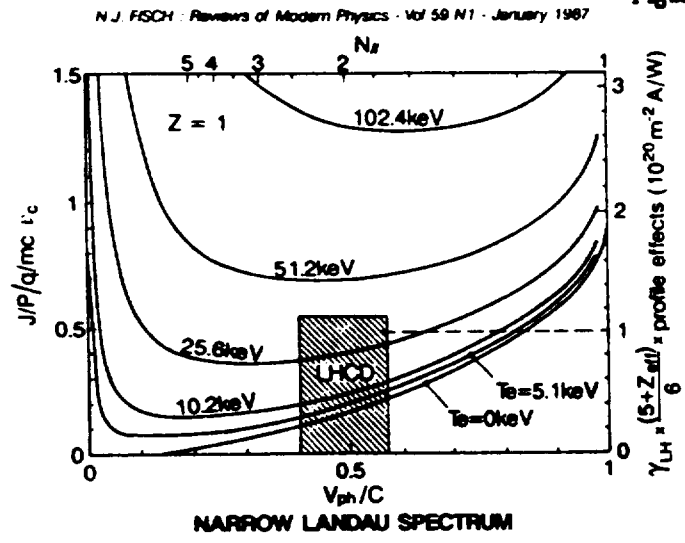

Figure 2

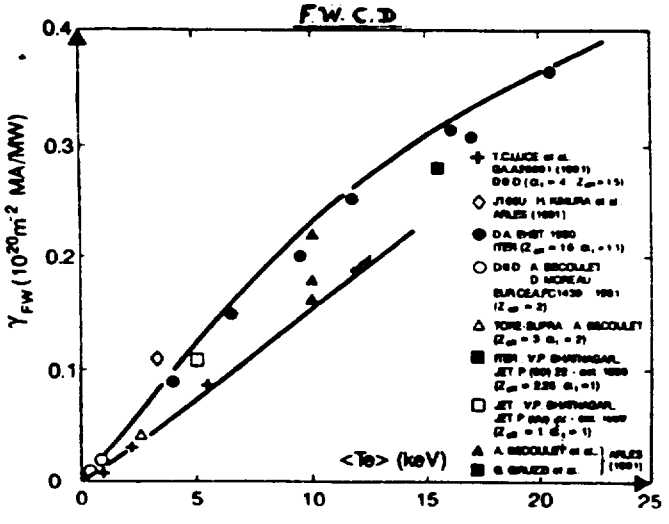

b)

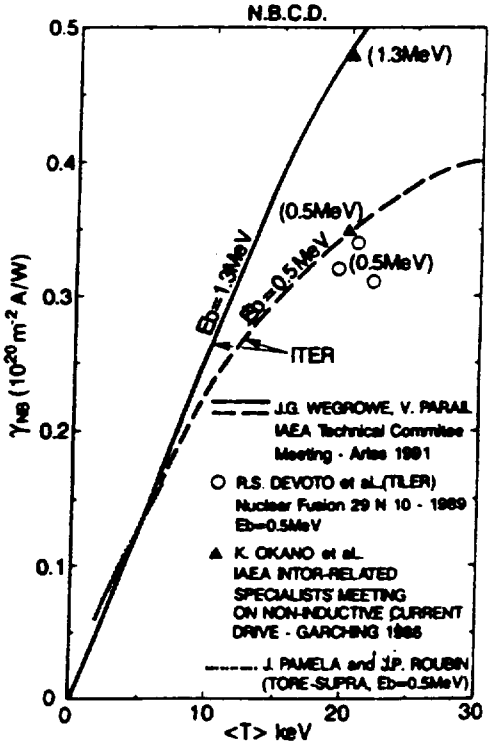

Figure 3 a)

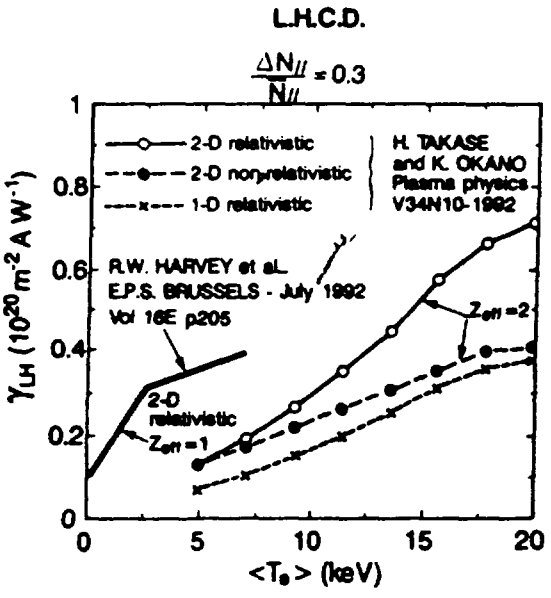

Figures 3 c)

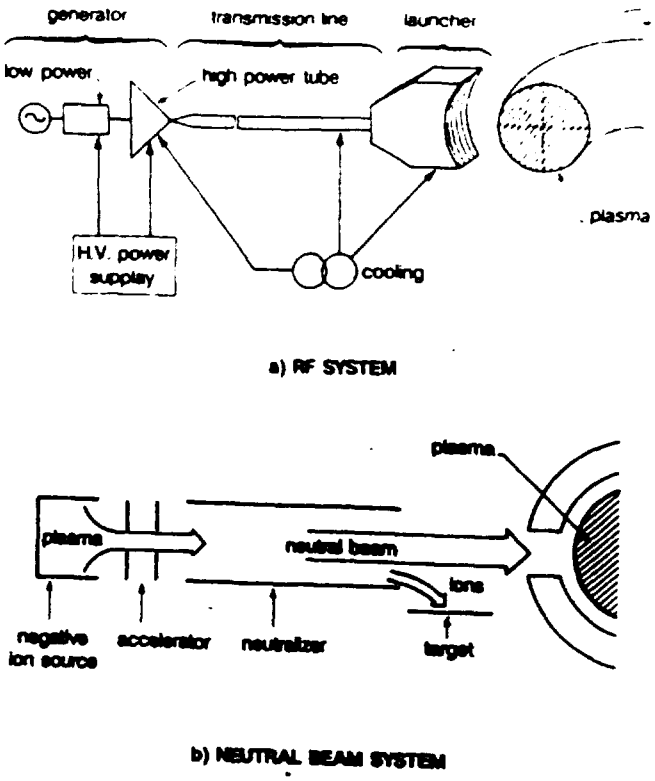

Figure 4

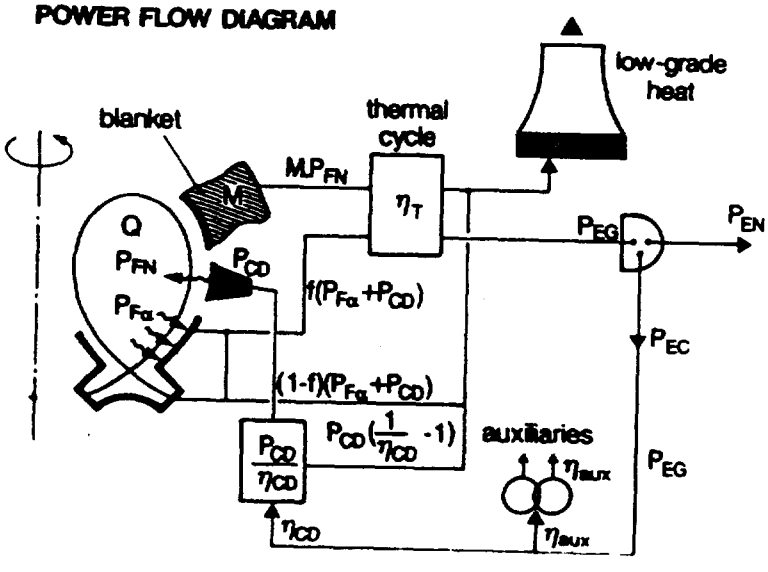

Figure 5

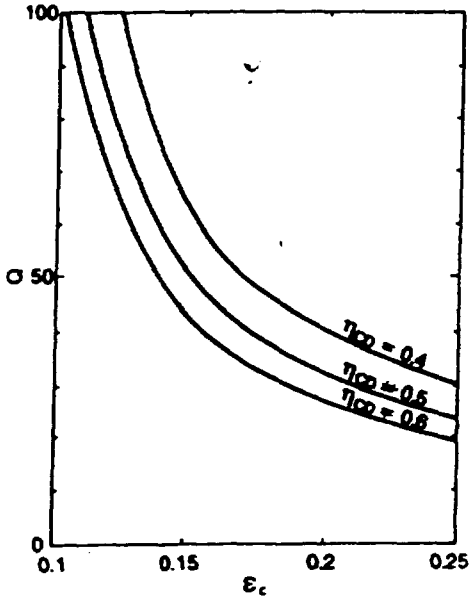

Figure 6

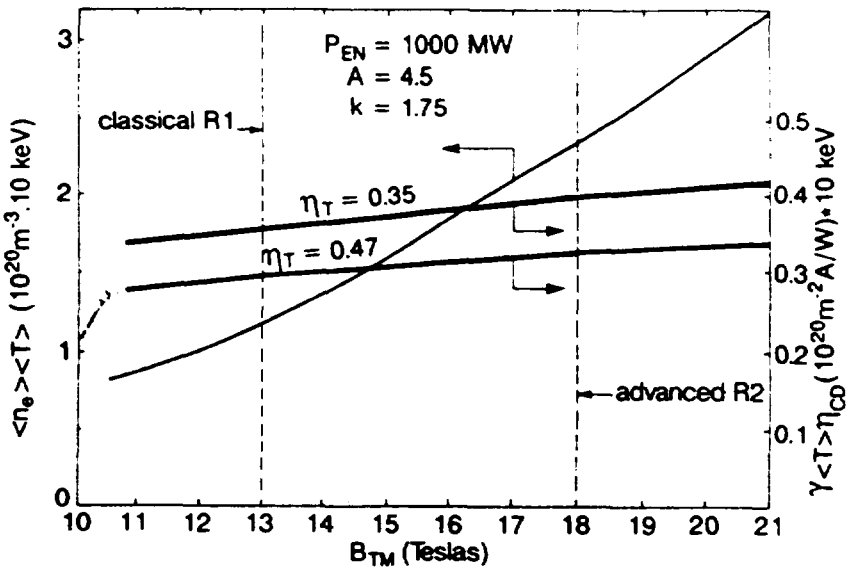

Figure 7

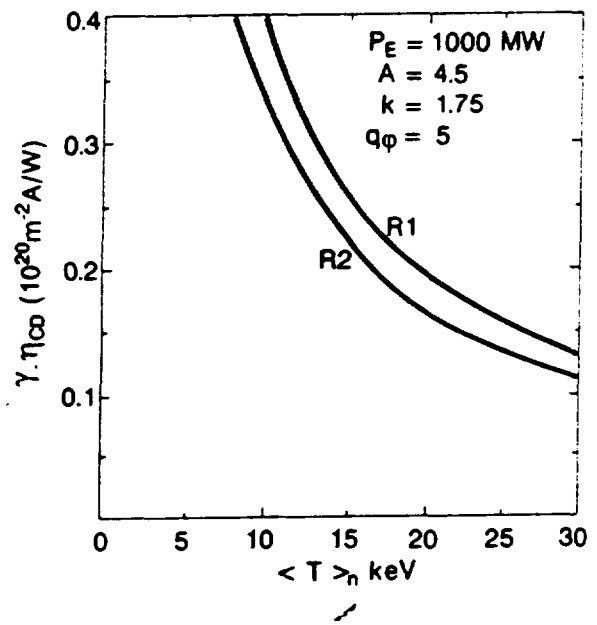

Figure 8

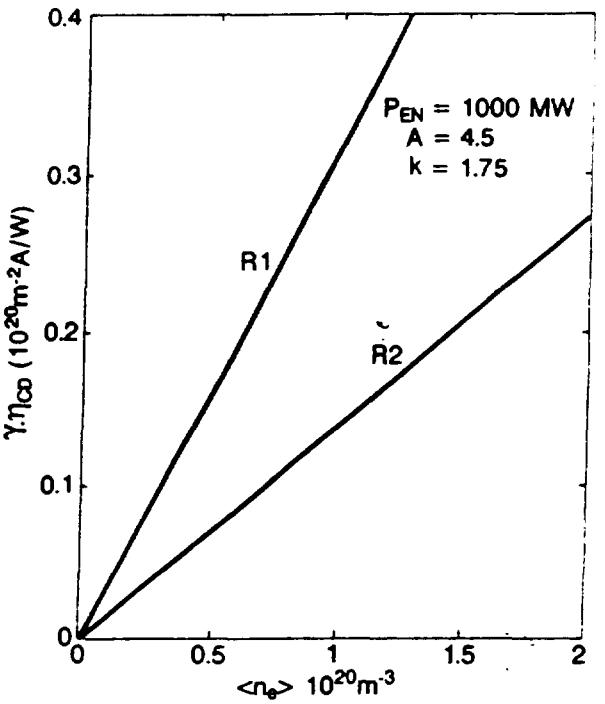

Figure 9

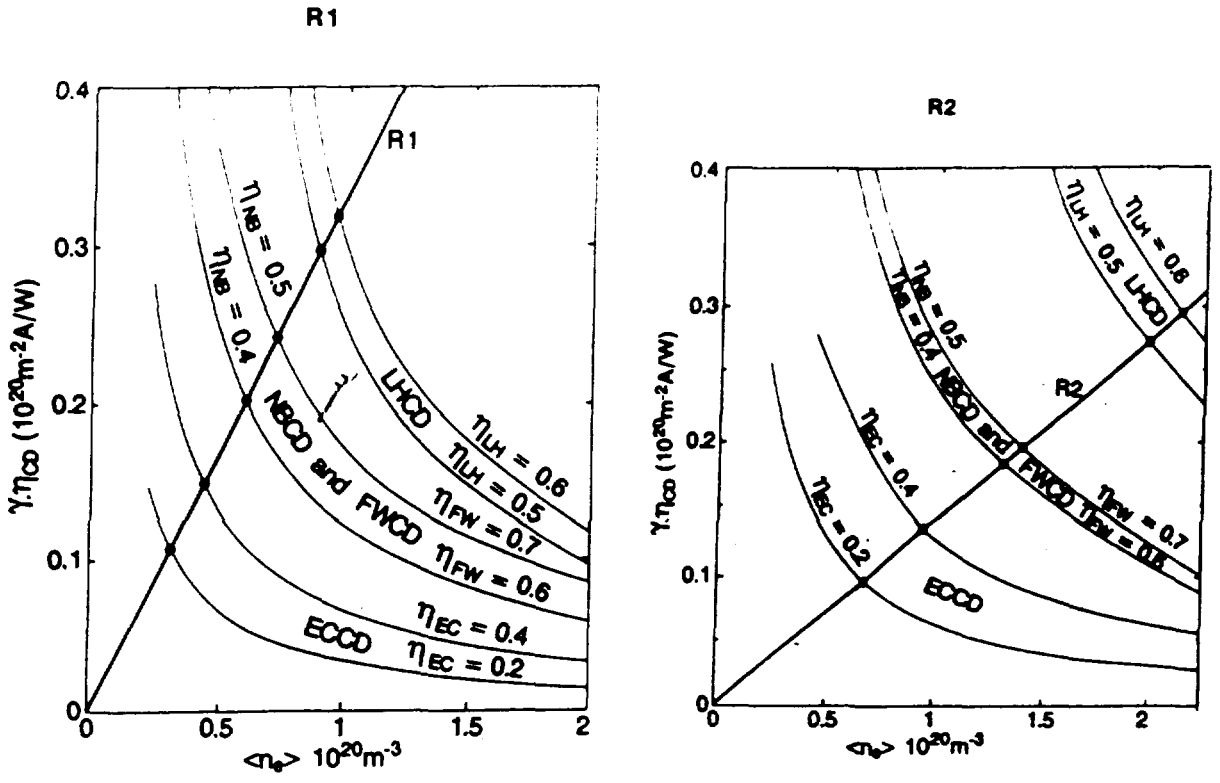

Figure 10

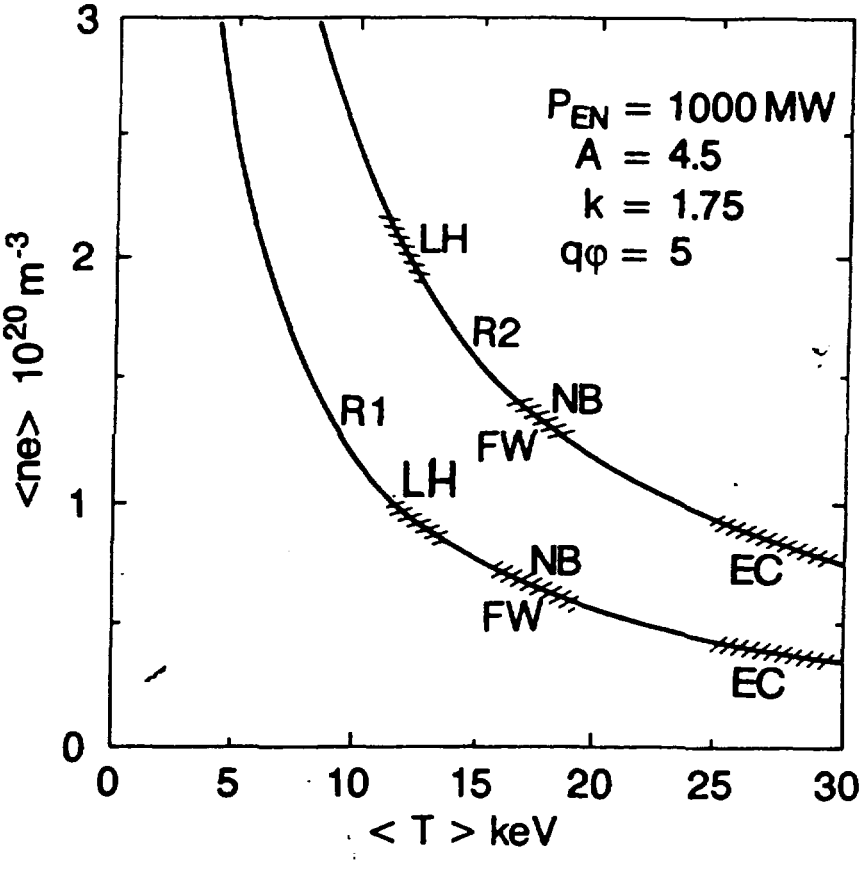

Figure 11